

The He abundance in NGC 1850 A and B: are we observing the early stage of formation of multiple populations in a stellar cluster?★

R. Carini,¹† A. Sollima² E. Brocato,^{1,3} K. Biazzo¹

¹INAF - Osservatorio Astronomico di Roma (OAR), via Frascati 33, 00078, Monte Porzio Catone (RM), Italy

²INAF-Osservatorio di Astrofisica e Scienza dello Spazio (OAS), Via Giobetti 93/3, 40129 Bologna, Italy

³INAF - Osservatorio Astronomico d'Abruzzo, via M. Maggini snc, I-64100 Teramo, Italy

Accepted for publication by MNRAS

ABSTRACT

We present the result of a sample of B-stars in the Large Magellanic Cloud young double stellar cluster NGC 1850 A and NGC 1850 B, observed with the integral-field spectrograph at the Very Large Telescope, the Multi Unit Spectroscopic Explorer. We compare the observed equivalent widths (EWs) of four He lines (4922 Å, 5015 Å, 6678 Å, and 7065 Å) with the ones determined from synthetic spectra computed with different He mass fraction ($Y=0.25, 0.27, 0.30$ and 0.35) with the code SYNSPEC, that takes into account the non-LTE effect. From this comparison, we determined the He mass fraction of the B stars, finding a not homogeneous distribution. The stars can be divided in three groups, He-weak ($Y < 0.24$) and the He-normal ($0.24 \leq Y \leq 0.26$) belonging to the MS of NGC 1850 A, and the He-rich stars ($0.33 \leq Y \leq 0.38$) situated in the MS associated to NGC 1850 B. We have analyzed the stellar rotation as possible responsible of the anomalous features of the He lines in the He-rich stars. We provide a simple analysis of the differences between the observed EWs and the ones obtained from the theoretical models with different rotation velocity ($V \sin i = 0$ and 250 Km/s). The resolution of the MUSE spectra do not allow to get a conclusive result, however our analysis support the He-enhanced hypothesis.

Key words: methods:observational – technique: spectroscopic – stars: abundances –galaxies:star clusters: individual: NGC 1850

1 INTRODUCTION

NGC 1850 is a young ($t_{age} \sim 90$ Myr; Niederhofer et al. 2015) and massive ($M \sim 5.5 \times 10^4 M_{\odot}$; Fischer et al. 1993) stellar cluster in the Large Magellanic Cloud (LMC), located at the edge of the galaxy bar. The cluster appears to be a binary system (NGC 1850 A and NGC 1850 B), and there is an indication of tidal interaction between the system members (Fischer et al. 1993). NGC 1850 B is located $\sim 30''$ W of the main cluster, constitutes $\sim 2\%$ of the total cluster population, and it is characterized by a significant younger age (between 4 Myr and 15 Myr, Fischer et al. 1993; Gilmozzi et al. 1994; Vallenari et al. 1994; Sollima et al. 2022). The color-magnitude diagram (CMD) of NGC 1850 A discloses a main sequence turn-off (MSTO) region that is wider than what is expected from a single stellar population and shows the presence of two main sequences (MSs): a blue and poorly populated MS, and a red MS which contains the majority of the stars. These features are not compatible with the typical photometric uncertainties, like field star contamination or differential reddening. (Bastian et al. 2016; Correnti et al. 2017; Milone et al. 2018).

The split of the MS and the extended-MSTO (eMSTO), have been observed in many young (age less 800 Myr and ~ 2.5 Gyr respectively) massive star clusters (YMCs) in the Magellanic Clouds (MCs)

(Milone et al. 2023). Unlike Galactic Globular Clusters (GGCs) in which the multiple populations observational evidences are mainly caused by star-to-star chemical abundance variations (e.g He, Na, O, see review by Bastian & Lardo 2018 and Gratton et al. 2019, Milone & Marino 2022 and reference therein), the YMCs of the MCs appears chemically homogeneous (e.g. Mucciarelli et al. 2014; Milone et al. 2020). The origin of the eMSTOs and the split MS is still debated. In the early works the eMSTO has been interpreted as the result of a prolonged star formation (e.g Mackey et al. 2008; Keller et al. 2011). Nowadays, stellar rotation has been suggested as the dominant cause of these photometric features (Bastian & de Mink 2009; D'Antona et al. 2015), however rotation effects do not fully reproduce the observed MSTOs of the entire sample of the CMD observed in the MCs (e.g Milone et al. 2017). As a consequence, some authors suggest that a mix of age variation and rotation could explain in a more effective way the eMSTOs and split MS phenomena (Goudfrooij et al. 2017; Costa et al. 2019). In the case of NGC 1850, Correnti et al. (2017) suggested that the combination of single stellar populations (SSPs) with an age range of ~ 35 Myr along with different rotation rates could explain the eMSTO and the MS split of the cluster.

Recently, Kamann et al. (2023) found rotation velocity differences along the blue and red MSs, with the blue arm primarily consisting of slow rotators (~ 100 Km/s), while the red arm mainly consists of rapid rotators (~ 200 km/s).

Until now, the phenomena of multiple stellar population in YMCs and in GGCs seems not sharing the same origin and cause.

By adopting the hypothesis of a dynamical association between

★ This paper is dedicate to the memory of Dr. Antonio Sollima, who passed away prematurely in 2023.

† E-mail: roberta.carini@inaf.it

NGC 1850 A and NGC 1850 B, this binary cluster seems to have the right mass and size to evolve in the next 10 Gyr toward the typical configuration of a present-day GC formed by two distinct stellar populations (Baumgardt & Hilker 2018). Thus, it exists the intriguing possibility that this cluster could serve as a unique bridge between the young massive stellar clusters observed during the formation of the multiple populations and the GCs exhibiting multiple populations observed some Gyr after their formation.

With the aim of better understanding the stellar populations in YMCs and their possible evolution toward a GC appearance, we analyze the chemical abundance in NGC 1850 A and NGC 1850 B.

The presence of He spread has been the main marker of multiple populations in GCs (eg. Cassisi et al. 2017; Gratton et al. 2019; Milone & Marino 2022 and reference therein). All the formation scenarios aiming to explain the origin of the multiple populations in GCs, predict that the second generation of stars are enhanced in helium. The difference in He abundance between stellar population can explain the peculiarities in the CMDs of the GGCs, as the main-sequence split and the morphology of the horizontal branch (see review Bastian & Lardo 2018; Gratton et al. 2019; Milone & Marino 2022 and reference therein). In fact, stars with higher helium, due to the higher molecular weight, evolve more rapidly, and are more luminous than lower helium models of the same mass, so the sequence of the He-rich models is bluer. Moreover, the different scenarios predict quite different He abundances at the end of the formation processes. For example, in the AGB (Asymptotic Giant Branch) scenario the maximum helium enhanced expected is of the order of 0.36-0.38 in terms of mass fraction (Siess 2010; Doherty et al. 2014), differently the fast-rotating massive star scenario predicts helium values up to ~ 0.8 (Chantereau et al. 2016). Therefore, the He abundance is clearly crucial to constrain the origin of the multiple populations.

The first direct spectroscopic measurement of highly He-enhanced stars ($Y \sim 0.34$) has been provided by Marino et al. (2014) analyzing the blue horizontal branch of the GGC NGC 2808.

Although helium is the second most abundant element in stars, estimates of helium abundance in stellar cluster are quite rare. Recently, Lagioia et al. (2019) found traces of He enhancement ($\delta Y \sim 0.01$) in the second population of star of four GC belonging to the SMC and showing ages in the range of ~ 6 –10 Gyr. Carini et al. (2020) estimated the He abundance of 10 star in the stellar cluster NGC 330 in the SMC, finding a mean value of $\langle \epsilon(\text{He}) \rangle = 10.93 \pm 0.05$, without evidence of star-to-star helium abundance difference. Li et al. (2023) found an He spread of $\delta Y \sim 0.06$ -0.07 in the MS dwarf stars in the old GC NGC 2110, in the LMC. We intend to tackle this puzzling scenario by evaluating the helium abundance in NGC 1850 A and B. In particular, we analyze the He abundance in the B-type stars, whose visible spectra are dominated by lines of He I and the Balmer series of hydrogen. These are rather hot, massive stars with effective temperatures in the range from 1.0×10^4 to 3.0×10^4 K and masses in the range from 2 to 20 M_{\odot} .

Here, we continue the line of research of Sollima et al. (2022), using the same set of data observed with the Multi Unit Spectroscopic Explorer (MUSE) integral field spectrograph in adaptive optics mode and the photometric parameters found by the authors during their analysis.

This paper is organized as follows. In Sec. 2 we describe the MUSE observations and data reduction, while the synthetic spectra are illustrated in Sec. 3. The data analysis, the determination of the He abundance, the uncertainties associated and the influence of the

stellar rotation on the He features are presented in Sec. 4. The final remarks are provided in the last Section.

2 OBSERVATIONS

We analyzed a set of cubes observed with the integral field spectrograph MUSE (Bacon et al. 2010; Kelz et al. 2016) at the Very Large Telescope (VLT) under the observing program 0102.D-0268(A) (PI: Bastian). The observations were conducted over a period of 6 nights between January and March 2019. Two fields were observed during each visit, namely a central field located at the cluster center (exposure time $t_{exp} = 2 \times 400s$) and an outer field ($t_{exp} = 3 \times 500s$) approximately 1 arcmin southeast of the cluster center, with a small overlap with the central field. The total exposure time per visit was 2300s. The data were obtained using the wide-field mode, with the ground-layer adaptive optics system activated. Each field of view is of 1×1 arcmin² with a spatial sampling of 0.2 arcsec. The wavelength range covered by the instrument is $\lambda = 4800$ -9300 Å with a low-to-medium resolution ($R \sim 1700$ -3500). Due to the emission of the laser guide star, the portion of spectrum between 5805 Å and 5965 Å has been masked. We downloaded the cubes reduced from the ESO Archive Science Portal¹. The six data cubes, containing flux and wavelength-calibrated spectrum in each spaxel, cover NGC 1850 A and B both visible in the right edge of the central point. Moreover, it was available the combined cube. This data set has already been used to determine the binary frequency on each of the arms of the split MS (Kamann et al. 2021) as well as to study the peculiar system NGC 1850-BH1 (Saracino et al. 2022; El-Badry & Burdge 2022), and the effect of the shell stars on the shape of the MSTO (Kamann et al. 2023). Sollima et al. (2022) determined the global metallicity on the basis of individual red supergiant (RSG) spectra ($\langle [M/H] \rangle = -0.31 \pm 0.01$), the Ba abundances ($\langle [Ba/Fe] \rangle = 0.4 \pm 0.02$) and the dynamical mass ($\log(M/M_{\odot}) = 4.84 \pm 0.10$) of the cluster. Moreover, the authors analyzed the O abundance among bright MS stars in NGC 1850. They found two groups of stars, the O-strong stars ($[O=Fe] = -0.16 \pm 0.05$) agrees with the value measured in stars with a similar metallicity in the LMC bar (Van der Swaelmen et al. 2013), and the O-weak stars displaying no O I triplet absorption lines. The authors interpreted this bimodality as evidence for different stellar rotation rates.

3 SYNTHETIC SPECTRA

In order to analyze the B stars spectra, we have computed detailed synthetic spectra with SYNSPEC, version 54 (Hubeny et al. 2021) using non-LTE (NLTE) line-blanked, model atmospheres of the grid *BSTAR2006* Lanz & Hubeny (2007) for early B-stars. We chose the non-LTE approach because many authors, (e.g. Auer & Mihalas 1973; Przybilla et al. 2005, 2006) have shown in their analysis how the LTE approach leads to erroneous abundance of He in B stars. The model atmospheres, calculated with TLUSTY (Lanz & Hubeny 2007), consider the 1D plane-parallel geometry, with hydrostatic and radiative equilibrium. The grid contains 16 effective temperatures $15000 \text{ K} \leq T_{eff} \leq 30000 \text{ K}$, with 1000 K steps, 10 surface gravities, $2.50 \leq \log g \leq 4.75$, with 0.25 dex steps and for 10 metallicities: 2, 1, 1/2, 1/5, 1/10, 1/30, 1/50, 1/100, 1/1000, and 0 times the solar metal composition. So that the grid is useful for studies of typical environments of massive stars: the Galactic center, the Magellanic

¹ <http://archive.eso.org/scienceportal/home>

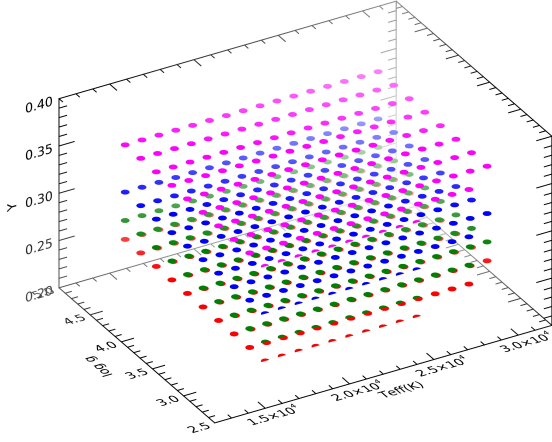


Figure 1. Grid points in the $\log g$ vs. T_{eff} vs Y plan. Red, green, blue and magenta points represent different He mass fraction Y , 0.25, 0.27, 0.30 and 0.35 respectively. For a colour version of the figure, see the electronic version of the paper.

Clouds, blue compact dwarf galaxies like I Zw-18, and galaxies at high redshifts. For model atmospheres, the grid is available at the TLUSTY Web site². Considering the typical characteristics of the star of NGC 1850, we adopt the stellar atmospheric models with $Z=0.008$ and microturbulent velocity of 2 Km/s. In fact, recent studies have determined the metallicity of the cluster, Sollima et al. (2022) and Song et al. (2021) found a value $[M/H] = -0.31$ ($Z \sim 0.008$), Kamann et al. (2023) found -0.33 . The standard solar abundances adopted are by Asplund et al. (2005).

The model atmospheres explicitly include, and allow for departures from LTE, 46 ions of H, He, C, N, O, Ne, Mg, Al, Si, S, and Fe, and about 53000 individual atomic levels grouped into 1127 superlevels. For more details see Hubeny et al. (2021); Lanz & Hubeny (2007) and reference therein. The triplet lines of He at 4922 Å are treated using special line broadening tables, in accordance with Barnard et al. (1974) Shamey (1969).

To have He enhanced synthetic spectra is not advantageous to construct a model from scratch, so we used the existing model from the grid to interpolate the values for the required helium abundance. A conservative estimate is to change the chemical abundance no more than 0.2 dex (Hubeny & Lanz 2017b). Since the difference in helium abundance between the populations could range from less than 0.01 to more than 0.2 in He mass fraction (Y) (e.g. D’Antona & Caloi 2004, Milone 2015, Gratton et al. 2019, Milone & Marino 2022 and reference therein), for each of these combinations in T_{eff} - $\log g$, models with a helium abundance of $\log N(\text{He})/N(\text{H}) = 0.00, +0.04, +0.1, \text{ and } +0.2$ dex were computed, corresponding with a helium abundance in mass fraction of $Y = 0.25, 0.27, 0.30$ and 0.35 .

The whole grid points are shown in Fig. 1, in the $\log g$ vs. T_{eff} vs Y plans.

To obtain a synthetic spectrum that is directly comparable to observations, one has to convolve the net emergent flux with the instrumental profile of the spectrograph that produced an observed spectrum to be analyzed. To this end, the synthetic spectra were degraded at

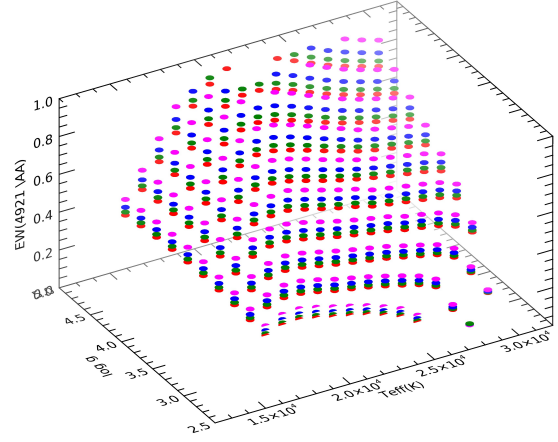


Figure 2. Equivalent width of the 4922 Å line in the $\log g$ vs. T_{eff} vs Y plan. The symbols are as in Fig. 1.

the MUSE resolution and normalized with ROTIN code (Hubeny & Lanz 2017a). For each spectrum, we have determined the equivalent width (EW) of 4 He absorption lines, at 4922 Å, 5015 Å, 6678 Å and 7065 Å. We omitted the most intensive He line at 5876 Å because it is not available in the MUSE spectra, since it falls in the portion of the spectrum masked. We obtained these values numerically integrating the normalized spectrum considering 10 Å-wide region on both sides of the He I lines. As example, in Fig. 2 we show the equivalent width of the 4922 Å line, calculated from the synthetic spectra.

As shown in Fig. 2 the behaviour of the intensity of the EW is in agreement with the theory. As expected:

- The EWs increases with the He abundance;
- Since lines of neutral helium first show up in the O-type stars, strengthen through the O-type stars, come to a maximum at a spectral type B2 on the main sequence, and the weaken toward later (cooler) type, the behaviour of the EWs has a maximum at 16000- 22000 K, and decreases for cooler and hotter temperatures;
- The intensity of the lines increases with the surface gravity.

Moreover, for values of T_{eff} less than 17000 K the strengths of this line are quite sensitive to temperature but relatively insensitive to gravity. For T_{eff} between 18000 K and 22000 K the abundance is dependent on $\log g$ more than T_{eff} . At still higher temperatures, both T_{eff} and $\log g$ must be accurately determined in order to derive the abundance of He from the measured equivalent widths (Wolf & Heasley 1985).

To compare the theoretical equivalent width (EW_{th}) with the observed ones (EW_{obs}), we have interpolated through the non-LTE grid of synthetic EWs as a function of T_{eff} and $\log g$.

4 DATA ANALYSIS

Spectra were extracted from the final MUSE data cubes using specifically developed software by Sollima et al. (2022) (for the details see Par 2 of the paper). The extraction was performed on each individual data cube, included the combined cube ($cube_{sum}$ hereinafter). We have extracted the spectra of the same 1167 stars from each cube. Residuals from the strong nebula emission lines were still visible in

² <http://tlusty.oca.eu/Tlusty2002/tlusty-frames-BS06.html>

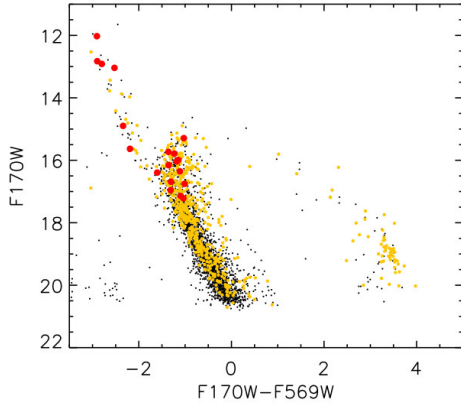


Figure 3. Color-magnitude diagram of the stars in the NGC 1850 area. Black points are the HST data, yellow points are the stars extracted from MUSE data cube, and the red point are the B stars analyzed here, of which we have determined He abundance.

some of the extracted spectra, but they do not affect the He lines. The region analyzed is not heavily influenced by nebulosity. In fact, analyzing the spectra of background in the regions nearby our selected stars, we have verified the absence of the He lines in emission. To identify the MUSE targets and to determine the effective temperature (T_{eff}) and gravity ($\log g$) of them we used the archival *Hubble Space Telescope* (HST) photometry of NGC 1850 taken with the Wide Field and Planetary Camera 2 (WFPC2) on March 4, 1994, during the program #5559 (PI: Gilmozzi). The data, reduced using *DOLPHOT* software (Dolphin 2000), include the images taken in three filters $F170W$, $F439W$ and $F569W$ and they have been already presented in Gilmozzi et al. (1994) and Sollima et al. (2022).

In Fig. 3 we show the color-magnitude diagram in $F170W$ and $F569W$ bands. The black points are the HST data, the yellow ones represent the MUSE targets extracted, the red ones are the B stars selected to estimate the He abundance (see Sec. 4.1). The MUSE sample covers a wide range of color and magnitude, it is possible to recognize the blue supergiants of NGC 1850 B ($F170W - F569W < -2$) the MS, RG and blue loop stars of NGC 1850 A ($F170W - F569W > -2$). A contamination from LMC stars is also present ($F439W - F569W > 0.3$ and $F569W > 17$, the magnitude in the band $F170W$ of these targets is not present in the catalog). Relevant quantities of the stars of our sample selected (see sect. 4.1) are reported in table 1, they were determined by comparing them with appropriate theoretical isochrones (see Sollima et al. (2022) for more details about this technique). We used Marigo et al. (2008)’s set of solar-scaled isochrones with a metallicity of $Z = 0.008$ and ages of 15 Myr, 90 Myr, and 10 G yr. Stars with the color $F170W - F569W < -2$ or stars within 5" from the center of the cluster NGC 1850 B to the youngest one, stars belong to NGC 1850 A are fitted with the isochrone at 90 Myr, and stars of LMC have been associated with the oldest isochrone. The distance modulus $(m - M)_0 = 18.50$ (Niederhofer et al. 2015) and the reddening $E(B - V) = 0.13$ (Górski et al. 2020) have been adopted. Once the T_{eff} and $\log g$ have been determined, the radial velocities of the targets stars have been derived by cross-correlating the stellar spectra with the appropriate and previously calculated synthetic spectra. Cross-correlation was performed using *fxcorr* task from *IRAF*, considering the available He

Table 1. Relevant quantities of the stars of our selected sample.

Id	Ra	Dec	T_{eff} (K)	$\log g$ (dex)	v_{rad} (Km/s)	$\sigma_{v_{rad}}$ (Km/s)
NGC 1850 A						
222	77.2163239	-68.7669383	15200	4.16	270	8
377	77.2080954	-68.7678015	15000	4.10	266	8
415	77.206	-68.761	20300	4.27	270	7
511	77.2018423	-68.7656164	16100	3.85	285	5
564	77.1990042	-68.7531787	17900	3.98	267	10
727	77.1924089	-68.7728569	16600	4.15	261	17
753	77.1915224	-68.7681341	15700	4.16	255	10
907	77.185	-68.774	16800	3.92	275	10
952	77.1835724	-68.7753472	16600	4.10	259	9
971	77.1830299	-68.770169	15800	3.98	280	11
1036	77.1795715	-68.7560604	15100	3.34	266	9
1069	77.1767874	-68.761876	16000	3.85	253	8
1129	77.1703261	-68.7598117	16800	3.77	235	7
NGC 1850 B						
605	77.1974417	-68.7680385	21400	4.27	254	6
1020	77.1805277	-68.7682749	25100	3.94	261	10
1077	77.1760504	-68.7641924	23000	4.20	257	9
1146	77.1673117	-68.7613749	29900	3.83	255	10
1153	77.1655824	-68.7616053	30000	3.62	262	8
1160	77.1639984	-68.7606044	28500	3.83	257	10
1161	77.1635335	-68.7617016	25800	3.83	269	8

lines. As noted by Sollima et al. (2022), the accuracy of the radial velocity varies greatly with the color of the targets, for this reason the values found for the B stars in this work are slightly different from the average velocity found by Sollima et al. (2022), Fischer et al. (1993) (251.4 ± 2 Km/s) and Song et al. (2021) (248.9 ± 2.5 Km/s), who have derived the radial velocity from a sample of RSG stars which are much cooler than the stars used here. Finally, we shifted the spectra to the rest frame.

4.1 Selection criteria for our sample of B stars in NGC 1850 A and NGC 1850 B

On the basis of the 1167 stars in our sample of MUSE spectra, we selected the stars with a T_{eff} between 15000 K and 30000 K, the surface gravity $\log g$ between 2.5 and 4.75, values of the theoretical grid (see Sec. 3). We also selected the ones with at least two available measurements of magnitude in the bands $F170W$, $F439W$ and $F569W$, this is to secure a fairly reliable determination of the T_{eff} for the stars included in the selected sample. In this way, we end up with a sample reduced to 232 targets.

Moreover, we excluded the Be stars to minimize uncertainties due to rotation and complexity in the spectra analysis, identified spectroscopically through the $H\alpha$ emission. We found a fraction of Be stars a little bit higher ($\sim 65\%$ of the sample) than one found in NGC 1850 by Bastian et al. (2017) ($\sim 20\text{-}50\%$) and in other young massive cluster Milone et al. (2018) (40-55 %).

We have also excluded the spectra showing stellar activity, the ones in which the He lines are too faint to be fitted or the signal to noise (S/N) is lower than 30. In conclusion, our selected sample is composed by 20 B stars, all these stars are highlighted as red point in Fig. 3. This sample includes B stars of NGC 1850 A and B as reported in table 1. For simplicity, we consider stars of NGC 1850 B

each target associated to the youngest isochrone, even if the distance from the center of the sub-cluster is more than 5".

4.2 He abundance

In this section, we make use of the spectral data secured by MUSE observations to evaluate the helium abundances in the B stars of NGC 1850 A and B, and to investigate the presence of a possible spread of this quantity in our sample.

4.2.1 EWs determination

To estimate the He abundance we determine the equivalent width of the lines at 4922 Å 5015 Å 6678 Å and 7065 Å from the spectra observed, these values are then compared with the theoretical ones.

For the middle B spectral types, the interpretation of the He I at 4921.9 Å is complicated by the blends with Si II at λ 4921.7 Å and with lines of Fe II and S II at λ 4923.9 Å. While for B0 and B1, O II lines at λ 4924.6 Å perturbs the red wing of He I λ 4921.9 Å. Moreover, middle and late B spectra are affected by S II at λ 5014.0 Å blending with He I at λ 5015.7 Å (Leckrone 1971). All these issues are well known, nevertheless we recall them to remind that the evaluation of He abundances in this range of wavelength has to be regarded with special care. For this reason, our results will be used to enlighten qualitative new discoveries which will lead to further work to be quantitatively confirmed.

In the present work, each He line was fitted individually to derive the EWs. As a first step, the continuum was estimated via a linear fit of the flux obtained in two narrow range (10 Å) of wavelength near the wings of each He absorbing line we intend to evaluate. This local continuum has been used to normalize the part of the spectra where it is present the He line.

The previous step make possible to evaluate the EW of each He line by performing a Gauss fit. As an example of the quite good quality of this step, Fig. 4 shows the best fit (red dashed line) obtained for the star #1146 at 4922 Å.

Unfortunately, the strongest line at 5876 Å has not been taken into account because the section of He line near the sodium doublet has been masked to avoid the strong emission due to the laser guide. It is relevant to report that none of these stars, but #971, exhibit a significant variation in radial velocity or in the EW values among the six epochs. This means that the stars of our sample can be considered single stars, or their companion is a low-mass star that does not significantly affect the radial systemic velocity. Since the S/N in the $cube_{sum}$ is systematically higher than the S/N found in each single $cube$, and the values of the mean EWs of each lines of the single cubes are in agreement, within the error, to the EW values of the $cube_{sum}$, we decide to continue the analysis only with the values estimated from the last one. In table 2, we present the EWs of the He lines at 4922 Å, 5015 Å, 6678 Å, and 7065 Å. Empty values in this table refer to features for which the best fit was not obtained, in most cases because the observed line was too weak or not detectable in the noise. In Fig. 5 we show the EW_{obs} (black points) for each star in each He I lines as function of temperature in comparison with the ones calculated with different helium mass fraction, $Y=0.25$ (red asterisks) and $Y=0.35$ (blue diamonds). For sake of clearness, the plot does not include the EW_{th} relative to $Y=0.27$ and $Y=0.30$. This figure shows a quite good agreement between the trend of the EW_{th} and the one of EW_{obs} as a function of T_{eff} . This result supports our previous assumption about the NLTE, which appears to be the most appropriate to analyse the helium abundance in B stars.

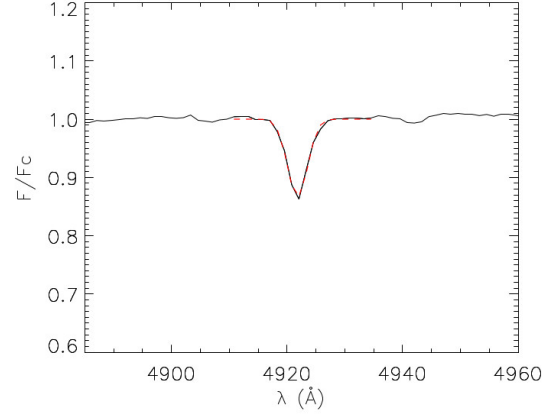


Figure 4. Best fit of the He line at 4922 Å for the star #1146. The black line is part of the spectrum extracted near the line, the red dashed line is the best fit.

4.2.2 He mass fraction evaluation

An evaluation of the He mass fraction (Y) from the EW_{obs} of the He lines can be obtained by using the synthetic computed for these lines. To this purpose we used a non-LTE grid of EW_{th} covering a wide range of effective temperature and gravity. The precise values of Y are then obtained by accurate interpolations through the non-LTE grid of EW_{th} for each line as a function of gravity, temperature and helium, when the measured quantities (EW_{obs}) are within the border values of the grid. In case the value is out of the available grid, we obtain a fair evaluation of the Y by using a linear extrapolation. We show an example of both the cases in Fig. 6 for the star #1146. The cyan point is the measured equivalent width from the MUSE spectrum while the black points are the values of the synthetic equivalent widths corresponding at $Y=0.25, 0.27, 0.30$ and 0.35 . The red lines represent the linear fit of the synthetic data.

Finally, we derived the He abundance by computing the mean of the abundances found for each available line, the results are reported in column 6 of the table 2 with the standard deviation associated (column 7). It is evident from our analysis that we can divide our sample in 3 groups, *He-normal* star, *He-weak* stars and the *He-enhanced* stars, or *He-rich*. Even if the typical He mass fraction value for LMC stars is $Y=0.25$, considering the uncertainties on the determination of the He abundance, we call *He-normal* stars the targets with Y between 0.24 and 0.26. The second group is populated by targets showing $Y < 0.24$, while the third is the sample collecting the stars with $Y > 0.26$.

We plot the targets of the three groups in the CMD with different symbols (fig. 7), it is evident that they arrange in specific part of the CMD:

- "*He-rich*" stars, with the exception the target #1069, are located in the region of the the MS associated to the isochrone at 15 Myr, with which we identify the NGC 1850 B cluster;
- Most of the "*He-normal*" stars (green diamonds) have a F170W magnitude larger than -2 mag, they are present only in the MS that collect the stars belonging to NGC 1850 A.
- The "*He-weak*" stars (light blue squares) seems to populate the reddest part of the MS (F170W lower than -2 mag).

According to (Osawa 1965; Garrison & Gray 1994) it is not surprising to find He-weak stars, because they constitute a sub-class

Table 2. Equivalent width (in Å) obtained from our analysis for each line and the derived mean Helium abundance (Y).

Star	EW ($\lambda 4921.9$ Å)	EW ($\lambda 5015.7$ Å)	EW ($\lambda 6678.2$ Å)	EW ($\lambda 7065.7$ Å)	$\langle Y \rangle$	$\sigma(Y)$
NGC 1850 A						
222	0.40 ± 0.04	0.19 ± 0.04	0.24	0.02
377	0.46 ± 0.04	0.17 ± 0.04	0.25	0.10
415	0.87 ± 0.07	...	0.52 ± 0.60	0.34 ± 0.06	0.26	0.01
511	0.39 ± 0.03	0.22 ± 0.04	0.30 ± 0.02	0.19 ± 0.03	0.20	0.05
564	0.63 ± 0.04	0.32 ± 0.02	0.43 ± 0.03	0.25 ± 0.04	0.24	0.08
727	0.52 ± 0.02	0.20 ± 0.04	0.40 ± 0.03	...	0.25	0.11
753	0.31 ± 0.06	...	0.22 ± 0.04	0.18 ± 0.04	0.18	0.10
907	0.41 ± 0.03	0.22 ± 0.03	0.26 ± 0.02	0.17 ± 0.02	0.10	0.06
952	0.52 ± 0.03	0.25 ± 0.08	0.26	0.06
971	0.33 ± 0.02	0.18 ± 0.06	0.13	0.06
1036	0.35 ± 0.02	0.20 ± 0.02	0.23 ± 0.01	...	0.16	0.06
1069	0.51 ± 0.04	0.25 ± 0.02	0.26 ± 0.02	0.23 ± 0.02	0.27	0.08
1129	0.52 ± 0.04	0.24 ± 0.06	0.22	0.02
NGC 1850 B						
605	1.04 ± 0.06	0.41 ± 0.03	0.54 ± 0.04	0.40 ± 0.04	0.38	0.09
1020	0.69 ± 0.03	0.27 ± 0.01	0.62 ± 0.03	...	0.36	0.07
1077	1.02 ± 0.08	...	0.55 ± 0.03	0.34 ± 0.04	0.33	0.08
1146	0.60 ± 0.02	0.24 ± 0.01	0.63 ± 0.04	0.43 ± 0.02	0.34	0.07
1153	0.42 ± 0.02	0.23 ± 0.01	0.62 ± 0.07	0.54 ± 0.03	0.34	0.11
1160	0.67 ± 0.02	0.24 ± 0.02	0.61 ± 0.02	0.41 ± 0.02	0.35	0.05
1161	0.67 ± 0.01	0.25 ± 0.01	0.63 ± 0.015	0.41 ± 0.02	0.37	0.07

of B-type stars. The He-weak stars have effective temperatures of typical B3-B5 stars, as in our sub-sample and the weak helium lines in the spectra of certain stars cause their spectral types to be inaccurately determined, leading to a discrepancy between their spectral type and their apparent color. Moreover, there is evidence that their spectra show variations in the metal lines and perhaps helium lines (Molnar 1972), as could be the case of the target #197 of our sample.

The He-rich targets (red points), are in the hot and bright part of the CMD, i.e. where the younger stars are located and in the region where we identify most of the stars of NGC 1850 B. On average the Y value of these stars is 0.35 ± 0.02 .

We note that 4 stars of this sub-sample are located at a distance from the center of NGC 1850 B less than 5", namely #1146, #1153, #1160, #1161. The other three are at larger apparent distance from the center, however a quick check by eyes shows they seem to lie in the edge between the two sub-clusters.

Quite interestingly we find that some of the He-rich stars are in common with the weak-Oxygen targets found by Sollima et al. (2022). If confirmed, this could be extremely interesting just because this kind of anti-correlations is quite typical of the multi-populations in Galactic GCs, in which the second generations of stars are rich in Helium and poor in Oxygen.

However, we remark that the two samples of stars (He-normal and He-rich) do not overlap in effective temperature, thus hampering a direct comparison and possibly leading to unknown sources of systematic error.

4.3 Uncertainties

The internal uncertainties on our He abundances include errors due to the determination of the atmospheric parameters. We evaluated the effective temperature and gravity of the B stars by comparing the theoretical models having the same color and magnitude of stars in our sample. The uncertainties on these quantities are dominated by the uncertainties on the magnitudes and distance. The photometric error of our data is about 0.02 mag (Gilmozzi et al. 1994). At the typical temperature of our sample, this translates to a temperature

uncertainty of ~ 1000 K and in gravity of ~ 0.01 dex. To estimate the internal uncertainties associated with the helium contents, we re-computed the abundance for a set of B stars varying the initial atmospheric parameters by (adding/subtracting) a quantity equal to their expected errors. By summing in quadrature the two contributions, we estimate the total uncertainty in Y as large as 0.04, being dominated by errors from temperature. Except for few stars, this evaluation of uncertainty appears smaller than the σ values estimated along the procedure of measuring the He abundance (see Tab 2).

A systematic error on the atmospheric parameters estimation could be due to the use of different grid models respect TLUSTY ones to convert the theoretical isochrones to the WFPC2 photometric system. In fact, Marigo and collaborators used the transformations primarily based on the LTE ATLAS9 (Castelli & Kurucz 2003) synthetic atmospheric models.

On this matter, we note that the LTE ATLAS9 and non-LTE TLUSTY model atmospheres both assume the same microturbulence, i.e. 2 Km/s^3 . Furthermore, Przybilla et al. (2011) tested the LTE ATLAS9 and NLTE TLUSTY model atmospheres, concentrating their work on the early-type stars of effective temperature between 15000 and 35000 K. They found that the temperature structure of the two models are in agreement, the differences are at most 1-2%, and they are even smaller for low metallicity. As a result of this work, they concluded that such a small difference is irrelevant for the stellar parameter determination. Moreover, Lanz & Hubeny (2007) compared the same models atmospheres for B stars. The authors find negligible differences between the continuum of the two spectra sets. The strongest difference is in the near ultraviolet range, where the LTE fluxes are about 10% higher than the NLTE predictions. This leads in a difference in the estimation of the effective temperature using HST broad bands lower than the uncertainties reported in our paper. We conclude that the use of the ATLAS9 models instead of TLUSTY ones does not affect the results of this work.

The possible systematic errors on the atmospheric parameters due

³ <https://wwwuser.oats.inaf.it/fiorella.castelli/grids.html>.

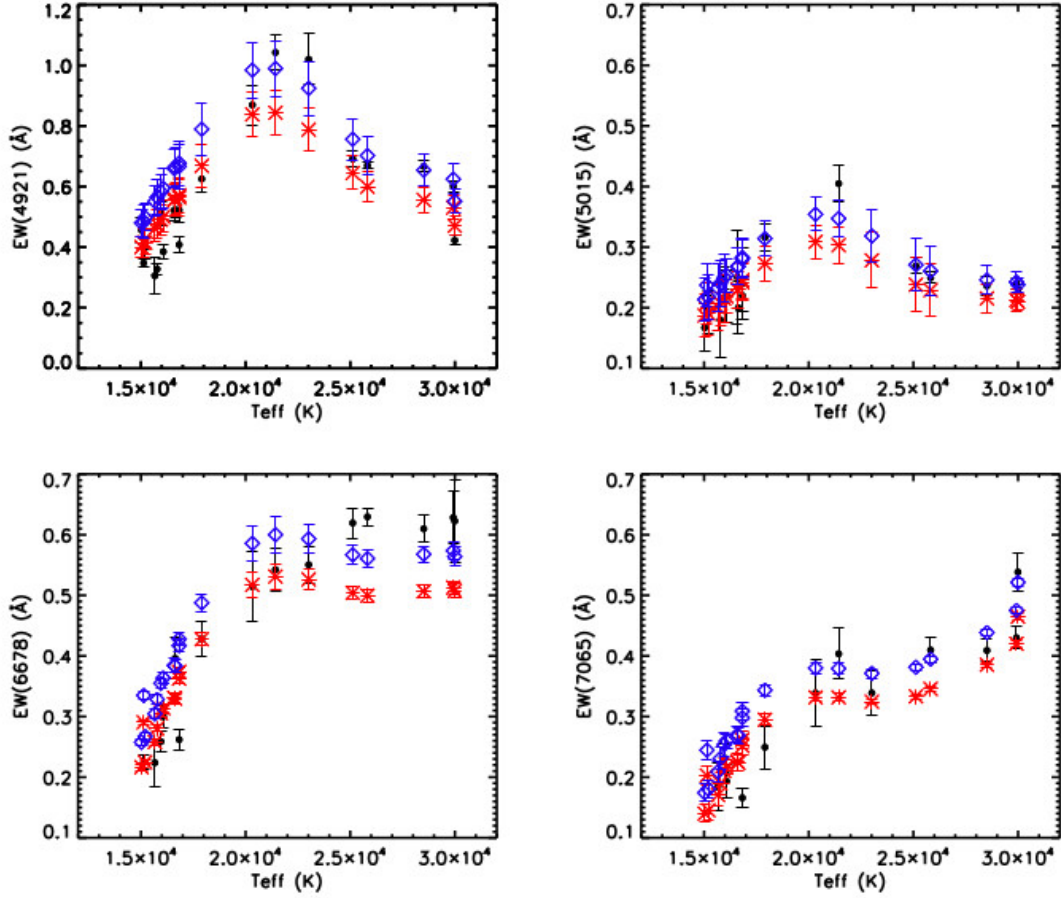


Figure 5. Equivalent width (\AA) for each line obtained from MUSE spectra (black dots) and from the interpolation of the theoretical EW_s with different helium mass fraction: red asterisk and blue diamonds for models with $Y=0.25$ and $Y=0.35$ respectively.

to the uncertainties in the adopted reddening have been also evaluated. To this purpose, we re-computed the temperature and gravity of each star by varying the initial reddening in an artificial way, i.e. by adding/subtracting to the original reddening of a quantity equal to their expected errors (0.015) (Górski et al. 2020). As a result, we have obtained mean differences in effective temperature about 200 K and in $\log g \approx 0.01$ dex, both values well within the uncertainties considered in this work.

Another source of systematic uncertainty could affect the He abundance is the microturbulence. Microturbulence is sensitive to the stellar atmospheric parameter, especially surface gravity (Hunter et al. 2007).

By analyzing spectra of 102 B stars, Lyubimkov et al. (2004) found that stars with mass between ~ 4 and $7 M_{\odot}$ have a microturbulence velocity (V_t) between 0 and 5 Km/s, with a average about 1.7 Km/s. While stars with mass in the range of $7 - 11 M_{\odot}$ have the same spread and average value of microturbulence of the previous case until their relative age t/t_{MS} is less then 0.8. After this value the microturbulence velocity could arise up to ~ 11 Km/s, with an average of about 7 Km/s. For the most massive stars ($12-18 M_{\odot}$) the microturbulence velocity spreads between 4 and 23 Km/s, and it

depends on the relative age t/t_{MS} .

Recently, Liu et al. (2022) found an empirical relationship between the microturbulence and surface gravity for the B-type stars:

$$V_t = -3.97 * (\log g)^2 + 17.85 * (\log g) - 2.52$$

The choice of 2 Km/s for our theoretical models is in agreements with the quoted studies, but for the hottest and massive ones #1146, #1153, #1160 #11161, for which the more accurate V_t should be about 7 Km/s. We believe that microturbulence may play a role in constraining the He abundance in young hot stars as the ones we studies here. Nevertheless, it does not seem that uncertainties of microturbulence can have an impact so sharp to generate the He-enhancement we found here.

4.4 Rotation

Since stellar rotation contributes to the broadening of line profiles in the stellar spectra, in this paragraph we discuss its possible role in the EWs values of the He lines in the NGC1850 B stars spectra. The aim is to understand if the increase of the EW_{obs} associated to the

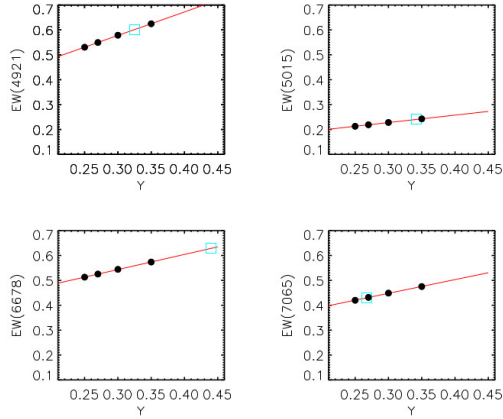


Figure 6. Values of the EW_{obs} (cyan square) and the EW_{th} (black points) corresponding at $Y=0.25, 0.27, 0.30$ and 0.35 , for the star #1146. The red lines represent the linear fit of the synthetic data.

The line profiles is due to the rotation or to the He-enhanced. Since the resolution of MUSE spectra is not high enough to analyze the issue in detail, we provide a qualitative analysis.

To find a plausible rotation velocity of B stars of NGC1850 B, we have compared the CMD with the isochrones of rotating models obtained from PARSEC version 2.0 (Nguyen et al. 2022). As an input indication for the age of these models, we took into account the work by Sollima et al. (2022) and Fischer et al. (1993) that fit the CMD of NGC 1850 B with a non-rotating isochrone of 15 Myr and 6 Myr respectively. Thus, we compare the HST photometry to 5 isochrones at 6 Myr and 15 Myr computed with different rotation rate $\omega = \Omega/\Omega_{cr}$ 0,0.6 and 0.9, where Ω is the angular velocity and Ω_{cr} is the breakup velocity, that is the angular velocity at which the centrifugal force is equal to the effective gravity at the equator. As shown in Fig. 7, the CMD of NGC 1850 B is pretty well fitted by all the isochrones taken into account, both rotating and non-rotating. By adopting these theoretical models, the stars having $F170W \sim -6$ are reproduced by isochrones of 6 Myr and 15 Myr and $\omega = 0.6$ disclosing equatorial velocity $v_{eq} \approx 230 - 250$ Km/s. On the other hand, if the isochrones with $\omega = 0.9$ are adopted, an equatorial velocity of $v_{eq} \approx 410$ Km/s is found.

Since velocities of 230-250 Km/s are derived for some stars of NGC 1850 B in the analysis by Kamann et al. (2023) and by Sollima et al. (2022), we decided to compute the theoretical spectra with ROTIN by assuming $Y = 0.25$ and a rotation velocity of 250 Km/s. Also in this case the synthetic spectra are degraded to the MUSE resolution and normalized. We considered the same set of T_{eff} and $\log g$ of the grid *BSTAR2006*. The same procedure explained in sec. 3 has been used to derive the EW_{th} of these models for each He lines. Since we are taken into account the case of $\Omega/\Omega_c = 0.6$, the effect of the rotation on the atmospheric parameters can be neglected (Frémat et al. 2005).

As an indicator of the quality of the derived EW_{th} , we determined the mean value of the difference ΔEW_{rot} between the EW_{th} evaluated from the synthetic models with rotation ($V \sin i = 250$ Km/s) and the observed ones. In this analysis we excluded the He-weak stars. The following results are obtained:

(i) $\Delta EW_{rot} = 0.04 \pm 0.04$ for NGC 1850 A

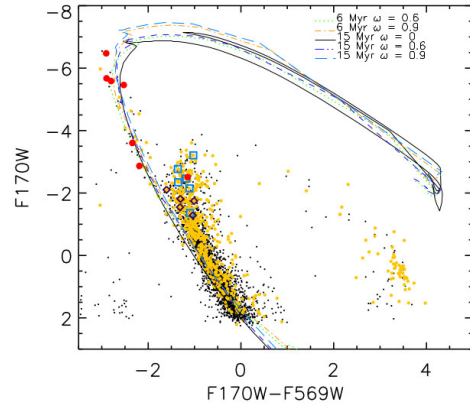


Figure 7. ($F170W-F569W, F170W$) CMD of NGC 1850 with superimposed isochrones with different rotation rate and age from Marigo et al. (2008) and Nguyen et al. (2022). Isochrones are colour-coded, in terms of their Ω/Ω_{cr} and age, as follows: $\Omega/\Omega_{cr}=0$ and age 15 Myr black line; $\Omega/\Omega_{cr}=0.6$ at 15 Myr purple dashed line; $\Omega/\Omega_{cr}=0.9$ at 15 Myr dark green long dashed line; $\Omega/\Omega_{cr}=0.6$ at 6 Myr green dotted line, $\Omega/\Omega_{cr}=0.9$ at 6 Myr cyan dash-dotted line. Targets associated with stars He-enhanced are marked by red dots.

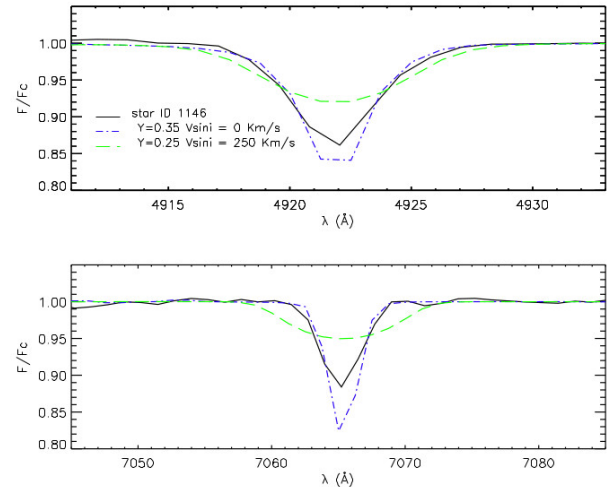


Figure 8. Spectra of the star #1146 (black line), in the range of wavelength around the He lines at ~ 4922 and 7065 . It is compared with the synthetic spectra calculated with $Y=0.35$ and $V \sin i=0$ Km/s (blue dot-dashed line), and with $Y=0.25$ and $V \sin i =250$ Km/s (green dashed line).

(ii) $\Delta EW_{rot} = 0.03 \pm 0.05$ for NGC 1850 B

In a fully similar way and including the same stars, we derive the mean difference between the EW_{th} estimated from the models with $V \sin i=0$ but Y different ($Y=0.25$ for the normal stars, $Y=0.35$ for the He-enhanced, but $Y=0.27$ for #1069), and the observed ones. In this case, we found the following values:

(i) $\Delta EW = 0.0007 \pm 0.03$ for NGC 1850 A

(ii) $\Delta EW = 0.002 \pm 0.050$ for NGC 1850 B

The comparison of the values of this indicator ($\Delta_{EW} \ll \Delta_{EW_{rot}}$) shows that the synthetic models without rotation provide a fit of the observed EWs of much better quality than the synthetic models with rotation. This can also be appreciated by eyes in Fig. 8, where we show the spectra of the NGC 1850 B star #1146 (black line) in the range of wavelength around two He I lines at 4922 (upper panel) and 7065 (lower panel). The two synthetic spectra are also plotted, they represent the results of the models with rotation and $Y=0.25$ (green dashed line), and without rotation but $Y=0.35$ (blue dot-dashed line). From this plot, it is evident that the model with rotation does not reproduce the wings and the depth of the He lines. Instead the He-enriched models fit well the wings of the lines, but are too deep. It is important to recall here that the resolution of the MUSE spectra is quite low and prevents a strong conclusion. A further intriguing possibility that could be confirmed or rejected by the analysis of high resolution spectra is briefly reported. Since fast rotation induces turbulent diffusion in the stellar interior, which drives the CNO-cycled material from the core to the envelope (Meynet & Maeder 2000), a possible hypothesis could be an He-enhanced (less than 0.35 in mass fraction) due to a stellar rotation (less than 250 Km/s).

5 CONCLUSIONS

In this paper we have examined for the first time the He abundance of B stars in the young (~ 90 Myr) binary LMC cluster NGC 1850. This system could be a unique bridge between two young massive stellar clusters observed during their process of formation of a multiple population and the old GCs exhibiting multiple populations.

We analysed the spectra of 20 B stars extracted by MUSE cubes.

To determine the He abundance, we compared the EWs of four He lines (4922 Å, 5015 Å, 6678 Å and 7065 Å) calculated from the MUSE spectra with the ones found analyzing the theoretical spectra.

These spectra has been computed with the code *SYNSPEC*, using non-LTE line-blanked model atmospheres of the grid *BSTARS2006* for early B-stars (Lanz & Hubeny 2007). We computed the model considering four different He mass fraction : 0.25, 0.27, 0.30, 0.35.

The results can be summarized as follows:

- We found a not homogeneous He abundance. In particular, we can divide the targets of our sample in three group: He-normal ($Y=0.25 \pm 0.01$), He-weak ($Y < 0.24$) and He-rich ($Y > 0.26$);
 - The last group is intriguing because all stars, but one, belong to the young isochrone, at 15 Myr, 4 of them are at a distance less than 5" from the center of NGC 1850 B, the other are in the edge between the two clusters. The mean value of the He mass fraction is about of 0.35 ± 0.02 .
 - Some He-rich stars are in common with the weak-O stars found by Sollima et al. (2022). If this is confirmed, e.g through the analysis of high resolution spectroscopy, it will be the first prove of anticorrelation in massive cluster in the MCs younger than 2 Gyr.
 - The He -normal and -weak stars are associated to the isochrone at 90 Myr.
 - We evaluated the effect of the rotation on the He abundance by computing synthetic spectra with $Y=0.25$ and $V \sin i = 250$ Km/s, in agreement with the works of Kamann et al. (2023) and with the v_{eq} values of the best isochrone that fit the CMD.
- From our qualitative analysis, the models without rotation but different Y fit better the EWs observed of NGC1850 B stars, but the resolution of the MUSE spectra is too low to have a strong conclusion.
- We highlight that unfortunately our sample of He-normal and He-rich stars do not overlap in effective temperature, thus hampering to quantify possible source of systematic errors.

In order to gain a deeper understanding of the characteristics or properties of the He features and clarify their nature, it is mandatory to perform high-resolution spectroscopic analyses (on which we will focus in future observational campaigns).

ACKNOWLEDGEMENTS

RC thanks Antonio Sollima, dearest friend, colleague and creator of this work. Sadly he passed away prematurely, before to see the final results. She thanks him for his advises and supports, but even more for his friendship, his joy, his humour, his music, his chats. She will be forever grateful to have had the opportunity to work together and to spent part of her life in his company.

This work is based on observations collected at the European Organisation for Astronomical Research in the Southern Hemisphere under ESO program 0102.D-0268(A) and made with the NASA/ESA Hubble Space Telescope and obtained from the Hubble Legacy Archive, which is a collaboration between the Space Telescope Science Institute (STScI/NASA), the Space Telescope European Coordinating Facility (ST-ECF/ESA) and the Canadian Astronomy Data Centre (CAD/C/NRC/CSA).

We thank the anonymous referee for the valuable comments and suggestions that improved the quality of the publication.

DATA AVAILABILITY

The data underlying this article will be shared on reasonable request to the corresponding author.

REFERENCES

- Asplund M., Grevesse N., Sauval A. J., 2005, in Barnes Thomas G. I., Bash F. N., eds, *Astronomical Society of the Pacific Conference Series Vol. 336, Cosmic Abundances as Records of Stellar Evolution and Nucleosynthesis*. p. 25
- Auer L. H., Mihalas D., 1973, *ApJS*, **25**, 433
- Bacon R., et al., 2010, in McLean I. S., Ramsay S. K., Takami H., eds, *Society of Photo-Optical Instrumentation Engineers (SPIE) Conference Series Vol. 7735, Ground-based and Airborne Instrumentation for Astronomy III*. p. 773508 ([arXiv:2211.16795](https://arxiv.org/abs/2211.16795)), doi:10.1117/12.856027
- Barnard A. J., Cooper J., Smith E. W., 1974, *J. Quant. Spectrosc. Radiative Transfer*, **14**, 1025
- Bastian N., Lardo C., 2018, *ARA&A*, **56**, 83
- Bastian N., de Mink S. E., 2009, *MNRAS*, **398**, L11
- Bastian N., et al., 2016, *MNRAS*, **460**, L20
- Bastian N., et al., 2017, *MNRAS*, **465**, 4795
- Baumgardt H., Hilker M., 2018, *MNRAS*, **478**, 1520
- Carini R., Biazzo K., Brocato E., Pulone L., Pasquini L., 2020, *AJ*, **159**, 152
- Cassisi S., Salaris M., Pietrinferni A., Hyder D., 2017, *MNRAS*, **464**, 2341
- Castelli F., Kurucz R. L., 2003, in Piskunov N., Weiss W. W., Gray D. F., eds, *Vol. 210, Modelling of Stellar Atmospheres*. p. A20 ([arXiv:astro-ph/0405087](https://arxiv.org/abs/astro-ph/0405087)), doi:10.48550/arXiv.astro-ph/0405087
- Chantereau W., Charbonnel C., Meynet G., 2016, *A&A*, **592**, A111
- Correnti M., Goudfrooij P., Bellini A., Kairai J. S., Puzia T. H., 2017, *MNRAS*, **467**, 3628
- Costa G., Girardi L., Bressan A., Chen Y., Goudfrooij P., Marigo P., Rodrigues T. S., Lanza A., 2019, *A&A*, **631**, A128
- D'Antona F., Caloi V., 2004, *ApJ*, **611**, 871
- D'Antona F., Di Criscienzo M., Decressin T., Milone A. P., Vesperini E., Ventura P., 2015, *MNRAS*, **453**, 2637
- Doherty C. L., Gil-Pons P., Lau H. H. B., Lattanzio J. C., Siess L., Campbell S. W., 2014, *MNRAS*, **441**, 582

- Dolphin A. E., 2000, *PASP*, **112**, 1383
- El-Badry K., Burdge K. B., 2022, *MNRAS*, **511**, 24
- Fischer P., Welch D. L., Mateo M., 1993, *AJ*, **105**, 938
- Frémat Y., Zorec J., Hubert A. M., Floquet M., 2005, *A&A*, **440**, 305
- Garrison R. F., Gray R. O., 1994, *AJ*, **107**, 1556
- Gilmozzi R., Kinney E. K., Ewald S. P., Panagia N., Romaniello M., 1994, *ApJ*, **435**, L43
- Górski M., et al., 2020, *ApJ*, **889**, 179
- Goudfrooij P., Girardi L., Correnti M., 2017, *ApJ*, **846**, 22
- Gratton R., Bragaglia A., Carretta E., D'Orazi V., Lucatello S., Sollima A., 2019, *A&ARv*, **27**, 8
- Hubeny I., Lanz T., 2017a, *arXiv e-prints*, p. [arXiv:1706.01859](https://arxiv.org/abs/1706.01859)
- Hubeny I., Lanz T., 2017b, *arXiv e-prints*, p. [arXiv:1706.01937](https://arxiv.org/abs/1706.01937)
- Hubeny I., Allende Prieto C., Osorio Y., Lanz T., 2021, *arXiv e-prints*, p. [arXiv:2104.02829](https://arxiv.org/abs/2104.02829)
- Hunter I., et al., 2007, *A&A*, **466**, 277
- Kamann S., Bastian N., Usher C., Cabrera-Ziri I., Saracino S., 2021, *MNRAS*, **508**, 2302
- Kamann S., et al., 2023, *MNRAS*, **518**, 1505
- Keller S. C., Mackey A. D., Da Costa G. S., 2011, *ApJ*, **731**, 22
- Kelz A., Kamann S., Urrutia T., Weibacher P., Bacon R., 2016, in Skillen I., Balcells M., Trager S., eds, *Astronomical Society of the Pacific Conference Series Vol. 507, Multi-Object Spectroscopy in the Next Decade: Big Questions, Large Surveys, and Wide Fields*. p. 323
- Lagioia E. P., Milone A. P., Marino A. F., Dotter A., 2019, *ApJ*, **871**, 140
- Lanz T., Hubeny I., 2007, *ApJS*, **169**, 83
- Leckrone D. S., 1971, *A&A*, **11**, 387
- Li C., et al., 2023, *ApJ*, **948**, 8
- Liu Z., Cui W., Liu C., Alexeeva S., Shi J., Zhao G., 2022, *ApJ*, **937**, 110
- Lyubimkov L. S., Rostopchin S. I., Lambert D. L., 2004, *MNRAS*, **351**, 745
- Mackey A. D., Broby Nielsen P., Ferguson A. M. N., Richardson J. C., 2008, *ApJ*, **681**, L17
- Marigo P., Girardi L., Bressan A., Groenewegen M. A. T., Silva L., Granato G. L., 2008, *A&A*, **482**, 883
- Marino A. F., et al., 2014, *MNRAS*, **437**, 1609
- Meynet G., Maeder A., 2000, *A&A*, **361**, 101
- Milone A. P., 2015, *MNRAS*, **446**, 1672
- Milone A. P., Marino A. F., 2022, *Universe*, **8**, 359
- Milone A. P., et al., 2017, *MNRAS*, **465**, 4363
- Milone A. P., et al., 2018, *MNRAS*, **477**, 2640
- Milone A. P., et al., 2020, *MNRAS*, **492**, 5457
- Milone A. P., et al., 2023, *A&A*, **672**, A161
- Molnar M. R., 1972, *ApJ*, **175**, 453
- Mucciarelli A., Dalessandro E., Ferraro F. R., Origlia L., Lanzoni B., 2014, *ApJ*, **793**, L6
- Nguyen C. T., et al., 2022, *A&A*, **665**, A126
- Niederhofer F., Hilker M., Bastian N., Silva-Villa E., 2015, *A&A*, **575**, A62
- Osawa K., 1965, *Annals of the Tokyo Astronomical Observatory*, **9**, 121
- Przybilla N., Butler K., Heber U., Jeffery C. S., 2005, *A&A*, **443**, L25
- Przybilla N., Nieva M. F., Heber U., Jeffery C. S., 2006, *Baltic Astronomy*, **15**, 163
- Przybilla N., Nieva M.-F., Butler K., 2011, in *Journal of Physics Conference Series*. p. 012015 ([arXiv:1111.1445](https://arxiv.org/abs/1111.1445)), [doi:10.1088/1742-6596/328/1/012015](https://doi.org/10.1088/1742-6596/328/1/012015)
- Saracino S., et al., 2022, *MNRAS*, **511**, 2914
- Shamey L. J., 1969, PhD thesis, University of Colorado, Boulder
- Siess L., 2010, *A&A*, **512**, A10
- Sollima A., D'Orazi V., Gratton R., Carini R., Carretta E., Bragaglia A., Lucatello S., 2022, *A&A*, **661**, A69
- Song Y.-Y., Mateo M., Bailey J. I., Walker M. G., Roederer I. U., Olszewski E. W., Reiter M., Kremin A., 2021, *MNRAS*, **504**, 4160
- Vallenari A., Aparicio A., Fagotto F., Chiosi C., Ortolani S., Meylan G., 1994, *A&A*, **284**, 447
- Van der Swaelmen M., Hill V., Primas F., Cole A. A., 2013, *A&A*, **560**, A44
- Wolff S. C., Heasley J. N., 1985, *ApJ*, **292**, 589

This paper has been typeset from a $\text{\TeX}/\text{\LaTeX}$ file prepared by the author.